PHYSICAL REVIEW B **83**, 241102(R) (2011)

Direct probe of Mott-Hubbard to charge-transfer insulator transition and electronic structure evolution in transition-metal systems

P. Olalde-Velasco,[1,2] J. Jiménez-Mier,[2,*] J. D. Denlinger,[1] Z. Hussain,[1] and W. L. Yang[1,†]
[1]*Advanced Light Source, Lawrence Berkeley National Laboratory, Berkeley, California 94720, USA*
[2]*Instituto de Ciencias Nucleares, UNAM, 04510 México Distrito Federal, Mexico*
(Received 6 June 2011; published 24 June 2011)

We report the most direct experimental verification of Mott-Hubbard and charge-transfer insulators through x-ray emission spectroscopy in transition-metal (TM) fluorides. The *p*-*d* hybridization features in the spectra allow a straightforward energy alignment of the anion-2*p* and metal-3*d* valence states, which visually shows the difference between the two types of insulators. Furthermore, in parallel with the theoretical Zaanen-Sawatzky-Allen diagram, a complete experimental systematics of the 3*d* Coulomb interaction and the 2*p*-3*d* charge-transfer energy is reported and could serve as a universal experimental trend for other TM systems including oxides.

DOI: 10.1103/PhysRevB.83.241102 PACS number(s): 71.20.−b, 71.27.+a, 78.70.En, 78.70.Dm

The emergent phenomena discovered in 3*d* transition-metal (TM) compounds, such as cuprates, manganites, cobaltates, and iron pnictides, have revolutionized our understanding of both fundamental physics and practical materials. In 1985, the seminal work of the Zaanen-Sawatzky-Allen (ZSA) diagram[1] was formulated to categorize the TM compounds. According to this diagram,[1–3] both the Coulomb interaction of the TM 3*d* electrons U_{dd} and the charge-transfer (C-T) energy between TM-3*d* and anion-*p* states $\Delta_{\text{C-T}}$ are important parameters for regulating the fundamental electronic structure. Two types of insulators, namely, Mott-Hubbard (M-H) and C-T insulators, are defined by comparing the value of U_{dd} with $\Delta_{\text{C-T}}$ (Fig. 1). Ever since, intensive experimental efforts have focused on deducing these key parameters;[2,4–21] however, a direct experimental result of a complete series of U_{dd} and $\Delta_{\text{C-T}}$ is still unavailable. Here, we present a systematic x-ray spectroscopic study on both the occupied and the unoccupied states of a series of TM difluorides (MF_2). The features from *d*-*p* hybridization enable a simple and self-consistent energy alignment through hybridization (EATH) for plotting TM-3*d* and anion-*p* states on a common energy scale, directly revealing the different types of insulators. With the data on both valence and conduction states, a complete and absolute experimental systematics of U_{dd} and $\Delta_{\text{C-T}}$ is further reported, in parallel with the theoretical ZSA diagram.

The significance of the ZSA diagram is that the valence states in the vicinity of the Fermi level could be from not only the TM-3*d*, but also the anion-*p* states (Fig. 1). This was later found to be the case for superconducting cuprates and has been providing an important foundation for studying 3*d*-TM systems (e.g., Ref. 22). Furthermore, the relative energy position of TM-3*d* and anion-*p* states in TM compounds has been one of the most important electronic structures that defines the performance of various devices, such as organic solar cells and lithium batteries.[23] Therefore, such a direct experimental probe is of both fundamental and technological importance; yet it has not been achieved due to the great technical challenge on determining the relative energy positioning of distinguished TM-3*d* and anion-*p* states.

Previous studies of the ZSA diagram in TM oxides and halides were mostly based on photoelectron spectroscopy coupled with theory, e.g., the line shape of the core-level photoelectron,[4–9] the valence-band photoelectron,[9–12] and the resonant photoemission[9,13–17] spectroscopies. Photoelectron spectroscopy probes total DOS, which inherently requires theoretical aid for resolving the TM 3*d*-DOS and anion 2*p*-DOS. The angle-resolved photoemission[18] is limited by the availability of conductive and cleavable single-crystal samples. Additionally, with few experimental results of inverse photoemission on NiO and MnO,[3,19,20] photoemission probes only occupied states and, thus, cannot provide direct experimental values of either U_{dd} or $\Delta_{\text{C-T}}$ because of the missing information on the energy levels of the unoccupied states.

X-ray absorption spectroscopy (XAS) and x-ray emission spectroscopy (XES) are bulk probes measuring both unoccupied and occupied states with the inherent elemental and orbital selectivity.[4] Previously, Ni-*L*,[21] oxygen-*K*,[24,25] and fluorine-*K* (F-*K*) (Refs. 26–28) edges were studied by either XAS or XES. However, the energy values of the spectra are in respect to the core levels of the particular elements. A complete experimental picture on the M-H to C-T transition, as well as the evolution of U_{dd} and $\Delta_{\text{C-T}}$, has never been achieved due to the lack of a method for obtaining the relative energy position of the *d* and *p* states and the difficulty in choosing an appropriate system.

The system we chose is 3*d*-TM difluorides, MF_2 with M = Cr–Zn. Our data show that MF_2 is a cleaner system for testing conceptual issues than oxides due to their extreme ionic status.[29] Additionally, MF_2 was only marginally studied.[8,12,26–28,30] There are still controversial questions on the type of insulators for the higher members in the series,[2,8,30] on the understanding of the fluorine XES line shape,[26,28,31] and on the irregular variation of the leading edges of XAS spectra.[26,27] All these questions are naturally answered in this Rapid Communication.

MF_2 samples were purchased from Sigma-Aldrich. Spectroscopic measurements were performed on the Beamline 8.0.1 at the Advanced Light Source (ALS). Experiments were performed at room temperature and with the linear polarization of the incident beam 45° to sample surfaces. The XAS spectra were collected in the total electron yield mode by registering the sample current normalized to the photon flux.

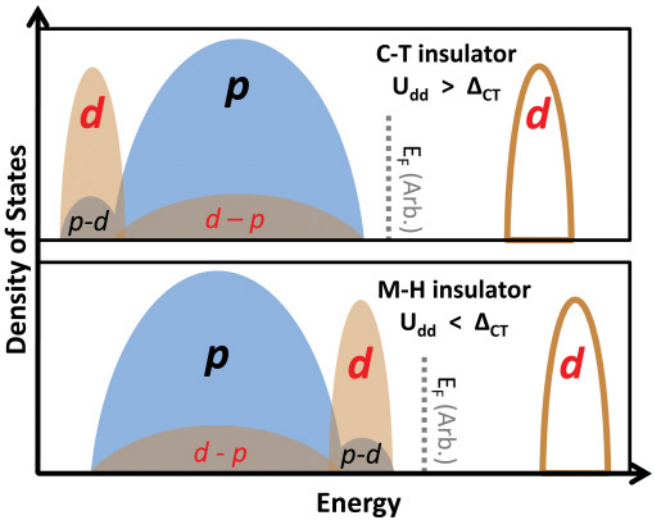

FIG. 1. (Color online) Schematic of (top) C-T and (bottom) M-H insulators. The lower intensity *d*-*p* and *p*-*d* humps are hybridization features in *d*- and *p*-partial DOS, respectively. Such features are evident in an MF_2 system, enabling a straightforward alignment of the experimental partial DOS of TM-3*d* with F-2*p*.

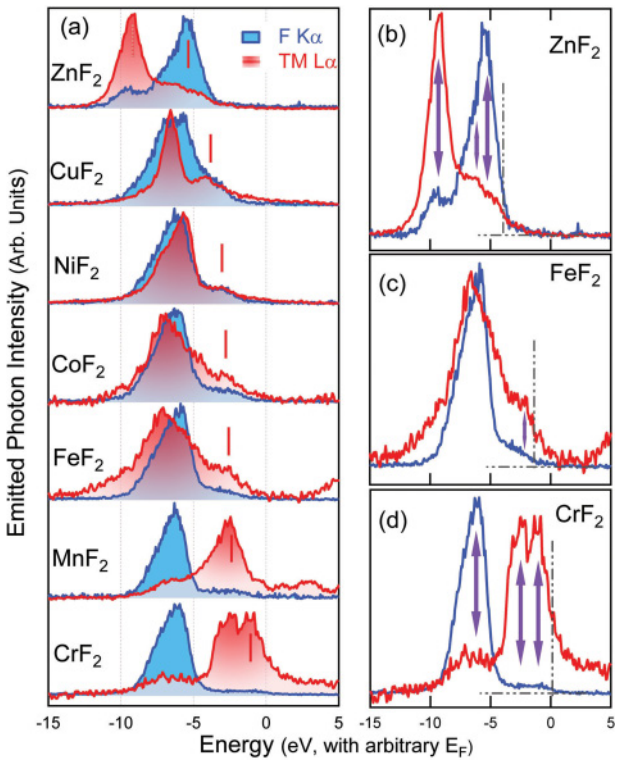

FIG. 2. (Color online) Experimental metal-3*d* and anion-2*p* valence states in MF_2 aligned by EATH. (a) XES spectra of TM-*Lα* in red (gray) and F-*Kα* in blue (black) displays the partial 3*d*- and 2*p*-DOS, respectively. The arbitrary intensity of the TM-*Lα* and F-*Kα* spectra are scaled to the same maximum value for each component. Bars are LHBs indicated by the highest-energy TM-3*d* peaks from top valence states. From CrF_2 to CuF_2, TM-3*d* LHBs shifts toward lower energy, in parallel with the shrinking of the hybridization shoulder in F-*Kα* spectra.[29] ZnF_2 is the only C-T or intermediate insulator with Zn-3*d* under F-2*p* valence states. (b)–(d) show three amplified examples on the energy alignments.[29] The leading edges of F-*K* and TM-*Lα*, the emission peaks of TM-*Lα* (F-*K*), and the hybridization features of F-*K* (TM-*Lα*), respectively, are aligned.

The XES spectra were obtained under nonresonant condition[4] with excitation energies of 600, 660, 730, 800, 880, 968.9, and 1094.1 eV for Cr-, Mn-, Fe-, Co-, Ni-, Cu-, and Zn-*L* edges. The resolution for XAS and XES measurements are 0.2 and 0.7 eV, respectively. All F-*K* spectra were collected in one experiment, with 700-eV excitation energy for XES measurements, to keep the relative energy shift reliable.

Our central result on the crossover of F-2*p* and TM-3*d* valence states in the MF_2 system is depicted in Fig. 2(a). Valence states from F-2*p* and TM-3*d* were measured through XES of fluorine-*Kα* (F-*K*) and TM-*Lα* (*M*-*L*), respectively.[4] Because only relative energy shifts are of interest here, the Fermi level was arbitrarily set at the leading edge of the spectrum of CrF_2. For F-2*p* states, the main peak position is almost stable from CrF_2 to ZnF_2. The most systematic change in the F-*K* line shape is on the high-energy shoulders at the −4- to 0-eV energy range, which is obvious in a magnified view [Figs. 2(b)–2(d), and Fig. S1 (Ref. 29)]. From CrF_2 to CuF_2, these shoulders shift toward the main peak with the intensity getting stronger mainly due to the closer position to the main peak. Nevertheless, for ZnF_2, this shoulder feature disappears, and a hump develops on the low-energy side of the main F-*K* peak, while a high-energy shoulder in *M*-*L* emerges simultaneously.

The shoulder and hump features in the MF_2 system, much clearer than that in oxides,[25,29] enables a straightforward way to align *M*-*L* with F-*K* XES spectra on a common energy scale, so the following conditions are met *simultaneously* for each component: (i) the leading edges of *M*-*L* are aligned to the leading edges of the F-*K* spectra; (ii) shoulders in F-*K* are aligned with peaks of *M*-*L* spectra; (iii) shoulders in *M*-*L* are aligned with peaks of F-*K* spectra. The consistency between the three types of alignments strongly suggests the validity of this energy alignment. For example, in Fig. 2(b), if the low- (high-) energy shoulder of F-*K* (*M*-*L*) in ZnF_2 is aligned with the main peak of *M*-*L* (F-*K*), the leading edges of F-*K* and *M*-*L* will be aligned simultaneously.

While the detailed discussion on the XES line shape is very complicated and is beyond the scope of this Rapid Communication, we focus on the energy position of the lower Hubbard bands (LHBs) that are defined by the top TM-3*d* valence states revealed by the highest-energy peak in *M*-*L* XES [bars in Fig. 2(a)]. The LHB is located on the higher-energy side of the corresponding F-2*p* state for CrF_2 to CuF_2 (M-H insulators) but evolves toward lower energy and eventually merges into the wide F-2*p* band for ZnF_2 (intermediate or C-T insulator). The consistency on the systematic evolution between the F-*K* shoulders and the *M*-*L* leading peak position (LHB) confirms that the shoulder and hump features originate from 3*d*-2*p* hybridization. This suggests the self-consistence of the EATH method and is in line with the schematic in Fig. 1.

In order to obtain a complete experimental picture on both the occupied and unoccupied states around the Fermi level, thus, U_{dd} and $\Delta_{C\text{-}T}$, we combined XAS of F-*K* edges with XES data in Fig. 3. Our XAS spectra are consistent with the recent

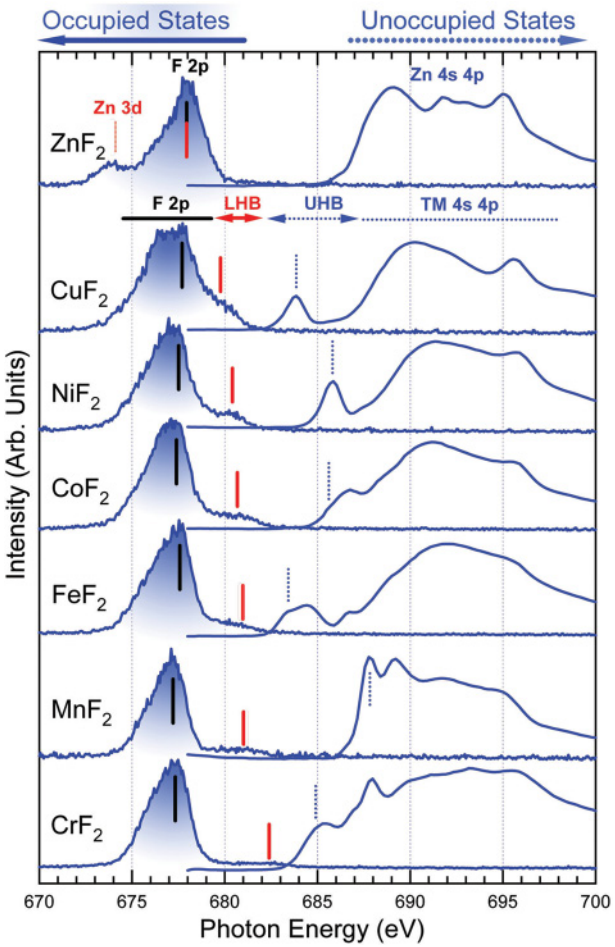

FIG. 3. (Color online) Fluorine-*K* XES and XAS experimental data plotted on a common energy scale. Red (gray) bars indicate LHBs from Fig. 2(a). Black bars indicate the highest-energy F-2*p* valence states. The TM-3*d* UHBs are defined by the lowest-energy intensity peaks in XAS data, the so-called in-gap states (dashed bars). The data exhibit monotonic energy shift on occupied F-2*p* and LHB states contrasting very irregular energies of unoccupied UHBs.

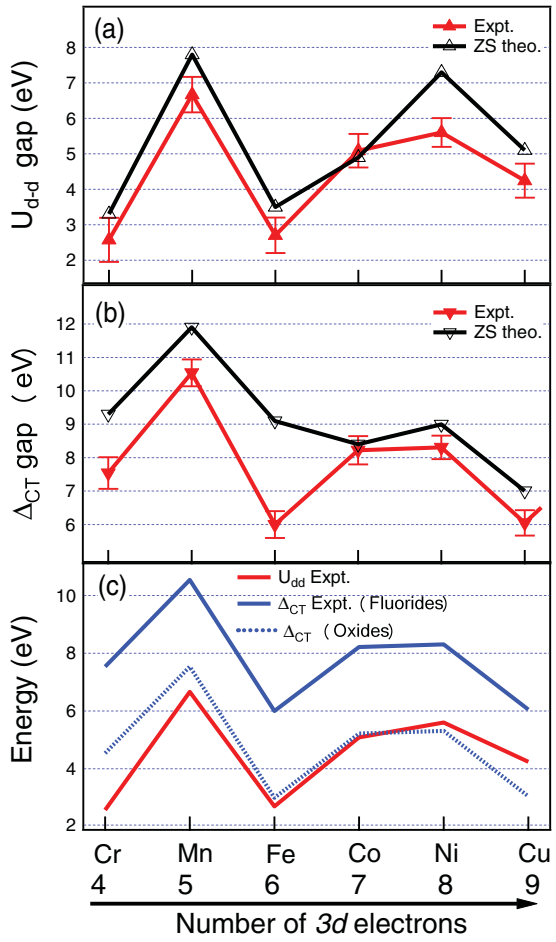

FIG. 4. (Color online) Systematics of U_{dd} and $\Delta_{C\text{-}T}$ generated from experiments on TM fluorides and their extension to oxides. (a) Experimental U_{dd} from Fig. 3 in comparison with theoretical Zaanen-Sawatzky (ZS) analysis. (b) Experimental and theoretical $\Delta_{C\text{-}T}$ basically follow the same trend as that of U_{dd}. (c) Direct comparison of experimental U_{dd} with $\Delta_{C\text{-}T}$ in difluorides and oxides. $\Delta_{C\text{-}T}$ were decreased by 3 eV for oxides to compensate the difference in electronegativity between F and O[2].

study on F-*K* XAS in difluorides.[27] Note that the band gap is indicated by the leading edges of XAS and XES, which is not a topic of this Rapid Communication. Here, we concentrate on the evolution of the highest-energy F-2*p* top valence states (black bars), LHB states [red or gray bars, from TM-3*d* in Fig. 2(a)], and upper Hubbard band (UHB) states defined by the lowest-energy peaks in XAS (dashed bars).

Figure 4 shows the summary of the experimental U_{dd} and $\Delta_{C\text{-}T}$ in MF_2 derived from Fig. 3, with values presented in Table S1 of Ref. 29. U_{dd}, ($\Delta_{C\text{-}T}$) is set as the energy difference between the red/gray (black) and dashed bars in Fig. 3, which corresponds to the theoretical energy value of the Hund rule ground-state term of $3d^x$ configurations.[2] For direct comparison, we also plotted the theoretical values from the ZS analysis.[2,29] The theoretical $\Delta_{C\text{-}T}$ for oxides was increased by 3 eV to compensate the difference on electronegativity between F and O, a method recommended by the original ZS analysis.[2] The most important physics is on the trend of the evolution.[2] The experimental and theoretical values of U_{dd} and $\Delta_{C\text{-}T}$ share the same trend from CrF_2 to CuF_2 (Fig. 4) except for FeF_2. The FeF_2 may contain contamination of Fe^{3+} as indicated by the XAS line shape;[24] however, the much lower experimental $\Delta_{C\text{-}T}$ of FeF_2 cannot simply be attributed to contamination because Fe^{3+} should display a much higher value of $\Delta_{C\text{-}T}$ as for MnF_2. This discrepancy calls for a theoretical revisit into the Fe^{2+} compound.

With the agreement between our experimental results and the theoretical ZS analysis,[2] we reached a complete understanding on the electronic structure evolution of MF_2 compounds. We first describe the occupied states through XES data. When we advance from lighter to heavier TM elements, the increasing nuclear charge enhances the binding energy of 3*d* electrons, leading to a monotonic decrease in *M*-*L* XES energy (Fig. 2). For the anion-2*p* states, F-2*p* here, the system is getting more covalent from CrF_2 to CuF_2, thus, less ionic and lower in binding energy. This effect is very small though because MF_2 remains a strong ionic system. The effect is exhibited by the broadening of the F-*K* XES main peak and

the monotonic but small (<1 eV) increase in XES energy (Fig. 2).

Second, contrasting the monotonic evolution of the occupied states in XES, the unoccupied states have to vary a great amount (Fig. 3) to accommodate the big changes in U_{dd} and $\Delta_{C\text{-}T}$ (Fig. 4). In general, the spatial extent of d orbitals shrinks with atomic number, leading to a trend of increasing U_{dd}. However, MnF_2 is a half-filled d^5 system, therefore, to add an electron to a high spin d^5 state means it has to go in with spin down, thus, there is no energy gain from the exchange. Such exchange stabilization leads to a sharp maximum at Mn^{2+} in both U_{dd} and $\Delta_{C\text{-}T}$ (Ref. 19) (Fig. 4). The decreasing U_{dd} from NiF_2 to CuF_2 is attributed to the spatially expanded d orbitals with increasing atomic radii from Ni (1.25 Å) to Cu (1.28 Å), which is due to the stronger electron-electron repulsion than the effect from increasing nuclear charges.

ZnF_2 is a special component in the MF_2 system. The 3d shell is full for Zn^{2+}, so there is no UHB. Our XES data (Fig. 2) show that the electron removal Zn-3d state is either merged into the broad F-2p bands (red bar) or deep below it (dotted bar), and only broad features corresponding to Zn-4s,4p hybridized with F-2p are observable in XAS (Fig. 3). Therefore, the first electron removal state is of F-2p character, and the first electron addition state is of Zn-4s,4p, a charge excitation from valence to conduction band involves a C-T process, thus, ZnF_2 is a C-T insulator with $\Delta_{C\text{-}T}$ of about 8.3 eV.

The reason that almost all MF_2 samples are M-H insulators is because fluorine is the most electronegative element, resulting in the lowest 2p level and the maximum C-T energy [Fig. 4(c)]. By a simple reduction of our experimental $\Delta_{C\text{-}T}$ by 3 eV to compensate the difference on electronegativity between F and O^2, a qualitative trend of $\Delta_{C\text{-}T}$ for TM oxides is generated. The derived $\Delta_{C\text{-}T}$, compared with the experimental U_{dd}, successfully displays a M-H to C-T insulator transition between CoO and NiO, leaving CuO as an obvious C-T insulator [Fig. 4(c)].

To summarize, this Rapid Communication provided a direct experimental probe of M-H and C-T insulators, and a pure experimental verification of the ZSA diagram. The reported experimental systematics of U_{dd} and $\Delta_{C\text{-}T}$ could serve as a general trend for other TM compounds. More importantly, the demonstrated EATH method will empower researchers to probe the relative energy position of TM-d and anion-p states, which is critical in various fields of material sciences.

We thank G. A. Sawatzky for his insight on data interpretation. The ALS at LBNL was supported by the US DOE under Contract No. DE-AC02-05CH11231. Work in Mexico was supported by Grants No. UNAM-PAPIIT IN109308 and No. CONACYT U41007-F CONACyT 56764. P.O. and J.J. acknowledge support from CONACyT Mexico. W.L.Y. acknowledges support from LDRD of LBNL.

*jimenez@nucleares.unam.mx

†wlyang@lbl.gov

[1] J. Zaanen, G. A. Sawatzky, and J. W. Allen, Phys. Rev. Lett. **55**, 418 (1985).

[2] J. Zaanen and G. A. Sawatzky, J. Solid State Chem. **88**, 8 (1990).

[3] J. Zaanen, G. A. Sawatzky, and J. W. Allen, J. Magn. Magn. Mater. **54-57**, 607 (1986).

[4] F. de Groot and A. Kotani, *Core Level Spectroscopy of Solids* (CRC Press Taylor & Francis, Boca Raton, FL, 2008).

[5] A. E. Bocquet, T. Mizokawa, K. Morikawa, A. Fujimori, S. R. Barman, K. Maiti, D. D. Sarma, Y. Tokura, and M. Onoda, Phys. Rev. B **53**, 1161 (1996).

[6] A. Kotani and K. Okada, *Recent Advances in Magnetism of Transition Metal Compounds* (World Scientific, Singapore, 1993).

[7] G. Lee and S. J. Oh, Phys. Rev. B **43**, 14674 (1991).

[8] J. Park, S. Ryu, M.-s. Han, and S. J. Oh, Phys. Rev. B **37**, 10867 (1988).

[9] M. Imada, A. Fujimori, and Y. Tokura, Rev. Mod. Phys. **70**, 1039 (1998).

[10] R. T. Poole, J. A. Nicholson, J. Liesegang, J. G. Jenkin, and R. C. G. Leckey, Phys. Rev. B **20**, 1733 (1979).

[11] R. T. Poole, J. D. Riley, J. G. Jenkin, J. Liesegang, and R. C. G. Leckey, Phys. Rev. B **13**, 2620 (1976).

[12] S. P. Kowalczyk, L. Ley, F. R. McFeely, and D. A. Shirley, Phys. Rev. B **15**, 4997 (1977).

[13] A. Fujimori *et al.*, Phys. Rev. B **42**, 7580 (1990).

[14] A. Kakizaki, K. Sugeno, T. Ishii, H. Sugawara, I. Nagakura, and S. Shin, Phys. Rev. B **28**, 1026 (1983).

[15] A. Tanaka and T. Jo, J. Phys. Soc. Jpn. **63**, 2788 (1994).

[16] S. J. Oh, J. W. Allen, I. Lindau, and J. C. Mikkelsen, Phys. Rev. B **26**, 4845 (1982).

[17] M. R. Thuler, R. L. Benbow, and Z. Hurych, Phys. Rev. B **27**, 2082 (1983).

[18] Z. X. Shen, C. K. Shih, O. Jepsen, W. E. Spicer, I. Lindau, and J. W. Allen, Phys. Rev. Lett. **64**, 2442 (1990).

[19] J. van Elp, R. H. Potze, H. Eskes, R. Berger, and G. A. Sawatzky, Phys. Rev. B **44**, 1530 (1991).

[20] G. A. Sawatzky and J. W. Allen, Phys. Rev. Lett. **53**, 2339 (1984).

[21] G. van der Laan, J. Zaanen, G. A. Sawatzky, R. Karnatak, and J. M. Esteva, Phys. Rev. B **33**, 4253 (1986).

[22] C. Weber, K. Haule, and G. Kotliar, Nat. Phys. **6**, 574 (2010).

[23] G.-A. Nazri and G. Pistoia, *Lithium Batteries Science and Technology* (Springer, New York, 2009).

[24] F. M. F. de Groot, M. Grioni, J. C. Fuggle, J. Ghijsen, G. A. Sawatzky, and H. Petersen, Phys. Rev. B **40**, 5715 (1989).

[25] E. Z. Kurmaev, R. G. Wilks, A. Moewes, L. D. Finkelstein, S. N. Shamin, and J. Kuneš, Phys. Rev. B **77**, 165127 (2008).

[26] C. Sugiura, J. Phys. Soc. Jpn. **60**, 2710 (1991).

[27] A. S. Vinogradov *et al.*, Phys. Rev. B **71**, 045127 (2005).

[28] E. I. Esmail and D. S. Urch, Spectrochim. Acta, Part A **39**, 573 (1983).

[29] See supplemental material at [http://link.aps.org/supplemental/10.1103/PhysRevB.83.241102] for figures of fluorides and oxides and values plotted in Fig. 4.

[30] K. Okada and A. Kotani, J. Phys. Soc. Jpn. **61**, 4619 (1992).

[31] A. S. Koster, J. Phys. Chem. Solids **32**, 2685 (1971).